Inorganic Chemistry

Article

pubs.acs.org/IC

Templating Influence of Molecular Precursors on $Pr(OH)_3$ Nanostructures

Eva Hemmer,[†,‡] Christian Cavelius,[‡] Volker Huch,[§] and Sanjay Mathur*[,∥]

[†]Institut National de la Recherche Scientifique—Énergie Matériaux Télécommunications, Université du Québec, 1650 Boulevard Lionel-Boulet, Varennes, Québec J3X 1S2, Canada

[‡]Leibniz Institute of New Materials, Im Stadtwald, Building D2 2, 66123 Saarbruecken, Germany

[§]Institute of Inorganic Chemistry, Saarland University, P.O. Box 151150, 66041 Saarbruecken, Germany

[∥]Institute of Inorganic Chemistry, University of Cologne, Greinstrasse 6, 50939 Cologne, Germany

Supporting Information

ABSTRACT: Four new praseodymium alkoxo and amido compounds ($[Pr_3(\mu_3\text{-}OtBu)_2(\mu_2\text{-}OtBu)_3(OtBu)_4(HOtBu)_2]$ (**1**), $[Pr\{OC(tBu)_3\}_3(THF)]$ (**2**), $[PrCl\{N(SiMe_3)_2\}_2(THF)]_2$ (**3**), and $[PrCl\{OC(tBu)_3\}_2(THF)]_2$ (**4**)) were synthesized and structurally characterized by single-crystal X-ray diffraction analysis. Application of these compounds in solvothermal synthesis of praseodymium oxide/hydroxide nanostructures showed their templating influence on the morphology and phase composition of the resulting solid-state materials. Differential reactivity of the chosen alkoxide ligands toward water and the different arrangements of metal−oxygen units in the studied precursor compounds strongly influenced the kinetics of hydrolysis and cross-condensation reactions as manifested in the morphological changes and phase composition of the final products. Thermal decomposition studies of **1**−**4** confirmed their conversion into the corresponding oxide phases. Activation of compounds **1**, **2**, and **4** by either a base or a stoichiometric amount of water showed the distinct influence of their chemical configuration on the obtained nanopowders: whereas **1** solely produced nanorods of $Pr(OH)_3$, **2** predominantly formed a mixture of rod-shaped and spherical particles. The solvothermal decomposition of **4** resulted in $Pr(OH)_2Cl$ or PrOCl due to the presence of Cl ligands in the molecular precursor. The resultant materials were thoroughly characterized to demonstrate the relationship between precursor chemistry and the processing parameters that are clearly manifested in the morphology and phase of the final ceramics.

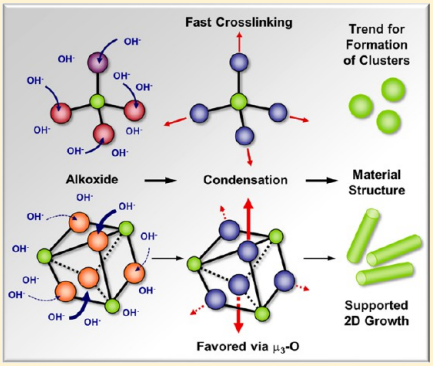

INTRODUCTION

The chemistry of lanthanide (Ln) elements continues to play a pivotal role in the development of both molecular and materials science.[1] Due to the outstanding optical and magnetic properties, the range of potential applications for lanthanide-containing materials is very wide ranging from phosphors for screens and monitors (Y_2O_2S, Tb−Gd_2O_2S) to solid-state laser materials (Nd:YAG) and biomarkers.[2] While lanthanide-doped solid-state materials are important for technological applications, molecular lanthanide complexes are sought for catalysis and medical diagnostics.[3] Control over the structure, reactivity, and solubility of the resulting lanthanide compounds by judicious choice and design of the ligands is an important thrust area of materials chemistry.[4] Herein, the precise knowledge about the precursor's molecular structure as well as the arrangement of ligands eases the achievement of such control. Furthermore, the bond closures and cleavages are intrinsic to the nucleation of a solid phase from a molecular source, and control over such atomic reorganization steps through chemical influence is not trivial. Targeted synthesis of inorganic materials poses significant challenges due to the multistep character, which often leads to inhomogeneities in composition, crystallite size, and microstructure. In addition, the supply of energy is generally empirically determined by analyzing snapshots of synthesis in terms of chemical composition and crystal structure. In this context, synthesis of advanced nanomaterials based on chemical homogenization techniques allows a controlled synthesis sometimes even outside the thermodynamically controlled regimes as reported for a wide variety of materials obtained through solution- or gas-phase processing of metal−organic precursors.[5]

Metal alkoxides of the lanthanides are potential precursors to oxide ceramics due to strong metal−oxygen bonds preexistent in the compounds.[4b,6] As hard Lewis acids[7] and due to the high contribution of ionic bonding, Ln^{3+} ions predominately saturate their coordination sphere via intermolecular linkages, resulting in oligomer rings or polymer chain structures. Consequently, simple alkoxides of lanthanide elements ($[Ln(OR)_3]_n$; R = −*i*Pr (isopropoxy), −Et (ethoxy), −Me (methoxy)) form clusters subject to the steric profile of attached alkyl groups and the propensity of alkoxide oxygen to act as a doubly ($-\mu_2$-) and/or

Received: March 7, 2015
Published: June 12, 2015

DOI: 10.1021/acs.inorgchem.5b00529
Inorg. Chem. 2015, 54, 6267−6280

Table 1. Details of the Crystallographic Data, Structural Determination, and Refinement for Compounds 1−4

	1	2	3	4
formula	$C_{44}H_{101}O_{11}Pr_3$	$C_{43}H_{89}O_4Pr$	$C_{16}H_{44}ClN_2OPrSi_4$	$C_{60}H_{124}Cl_2O_6Pr_2{\cdot}0.5C_4H_8O$
M, g mol^{-1}	1228.98	811.05	569.25	1330.36
T, K	100(2)	293(2)	100(2)	293(2)
wavelength, Å	0.71073	0.71073	0.71073	0.71073
space group	$P2_1/c$	$P\bar{1}$	$P2_1/n$	$P\bar{1}$
a, Å	19.869(4)	12.184(2)	14.2378(5)	13.076(9)
b, Å	10.882(2)	13.109(3)	13.0890(4)	17.170(11)
c, Å	27.854(6)	16.942(3)	16.4860(5)	18.606(8)
α, deg	90	68.61(3)	90	114.89(6)
β, deg	100.016(8)	87.86(3)	114.8860(10)	96.84(7)
γ, deg	90	62.63(3)	90	101.99(7)
V, Å ^{3}	5931(2)	2209.3(8)	2787.03(15)	3605(4)
Z	4	2	4	2
D_c, Mg m^{-3}	1.357	1.219	1.376	1.226
μ, mm^{-1}	2.024	1.139	2.470	1.451
R1^a/wR2^b (final)	0.0298/0.0600	0.0675/0.1807	0.0172/0.0420	0.0707/0.1522
R1^a/wR2^b (all data)	0.0386/0.0659	0.0701/0.1830	0.0205/0.0446	0.1896/0.1809

^{a}R1 = $\sum||F_o| - |F_c||/\sum|F_o|$. ^{b}wR2 = $[\sum w(F_o^2 - F_c^2)^2/\sum w(F_o^2)^2]^{1/2}$.

triply (μ_3-) bridging ligand.[8] Aiming for steric control, aryloxides or phenoxides as well as alkyl alkoxides of bulkier steric profile have been reported as suitable ligands.[9] For example, the introduction of sterically demanding alkoxo ligands such as *tert*-butoxy (−O*t*Bu) favors the formation of trinuclear structural units as reported by Bradley et al.[10] and Veith et al.[11] for lanthanum and yttrium alkoxides of general formula $[M_3(OtBu)_9(HOtBu)_2]$. Gromada et al. described the synthesis of neodymium alkoxide $[Nd_3(OtBu)_9(HOtBu)_2]$, while crystal data were reported for isostructural $[Nd_3(OtBu)_9(THF)_2]$.[12] Misra et al. reported the synthesis of *tert*-butoxy derivatives of Pr and Nd by alcoholysis of isopropoxides;[13] however, no investigations were made regarding the molecular structure of the complexes. Furthermore, due to the possible cleavage of the C−O bond and resulting favored bridging of several metal centers by oxo ligands (O^{2-}), formation of polynuclear oxo complexes cannot be completely excluded even when using bulkier *tert*-butoxy ligands as shown by Hubert-Pfalzgraf for the oxo cluster $[Pr_4O_3(OtBu)_6]_m$ formed in the reaction of $[Pr\{N(SiMe_3)_2\}_3]$ with BuOH.[14] Details on the formation of the oxo ligands or the formation mechanism were not provided. Also, synthesis of praseodymium *tert*-butoxide is reported in the literature,[15] but the crystal structure could not be determined.[16]

Among the lanthanides, praseodymium exhibits excellent optical characteristics manifested in several interesting praseodymium complexes of high luminescence efficiency or for applications as color pigments and in near-infrared reflective coatings.[17] Moreover, praseodymium forms oxides with variable valence states (3+ and 4+) such as Pr_2O_3, PrO_2, and Pr_6O_{11} that are stable under ambient conditions, making them promising functional oxide materials. For instance, Pr_2O_3 is a desired candidate for microelectronic applications due its high dielectric constant.[18] Furthermore, the variety of stable phases enables fast changes in the oxidation state of praseodymium, resulting in the highest oxygen ion mobility within the series of lanthanide oxides and making these oxides very attractive as catalysts.[19] In this context, various approaches have very recently been suggested for the synthesis of praseodymium oxide nanostructures, among them the synthesis of Pr_6O_{11} nanorods by annealing of $Pr(OH)_3$.[20] Aiming for the development of new suitable precursors for the preparation of functional praseodymium-based nanomaterials, in this work, $[Pr_3(OtBu)_9(HOtBu)_2]$ (**1**) was synthesized and the crystal structure was described for the first time. In addition, various heteroleptic praseodymium amide and alkoxide complexes ($[Pr\{OC(tBu)_3\}_3(THF)]$ (**2**), $[PrCl\{N(SiMe_3)_2\}_2(THF)]_2$ (**3**), and $[PrCl\{OC(tBu)_3\}_2(THF)]_2$ (**4**)) were isolated, and their suitability in the solvothermal synthesis as precursors to nanoscopic praseodymium hydroxides was investigated.

EXPERIMENTAL SECTION

General Procedures. All manipulations were performed in vacuum and in a nitrogen atmosphere using a modified Schlenk assembly. Organic solvents used for amide and alkoxide synthesis were purified and dried by standard procedures and stored over sodium or molecular sieves. CHN analysis was performed with a Vario Micro Cube by Elementar Analysen Systeme, Hanau, Germany. ^{1}H and ^{13}C NMR spectra were recorded on a Bruker AC 200 spectrometer (300 MHz for ^{1}H, 300 MHz for ^{13}C). The decomposition behavior of compounds **1**−**4** was investigated by differential thermogravimetry/differential thermoanalysis (TG/DTA) studies in 60 sccm of nitrogen using a TGA 1500 by Bähr with a heating rate of 10 K/min.

Synthesis of $[Pr\{N(SiMe_3)_2\}_3]$. $LiN(SiMe_3)_2$ used in the synthesis of the precursor $[Pr\{N(SiMe_3)_2\}_3]$ was obtained by reaction between *n*-butyllithium (477.0 mmol, 300 mL, 1.6 M in hexane, Acros Organics) and hexamethyldisilazane (477.0 mmol, 100 mL, Fluka, >98.0%) at room temperature for 24 h. The white powder was purified by sublimation at 80 °C ($p \approx 10^{-3}$ mbar) before further use. Yield: 92%, 73.1 g. Subsequently, the praseodymium precursor was synthesized by reacting stoichiometric amounts of $LiN(SiMe_3)_2$ (10.0 g, 60.0 mmol) and $PrCl_3$ (4.9 g, 20.0 mmol, Sigma-Aldrich, powder, water-free, 99.9% dried under dynamic vacuum ($p \approx 10^{-3}$ mbar) at 120 °C for at least 1 h and activated by THF (50 mL) at 60 °C for 2 h) in toluene as described in the literature.[21] The obtained light green powder was purified before further use by sublimation at 130 °C ($p \approx 10^{-3}$ mbar). Yield: 92%, 11.6 g. Anal. Calcd for $[Pr\{N(SiMe_3)_2\}_3]$: C, 34.8; H, 8.8; N, 6.8. Found: C, 34.5; H, 8.8; N, 6.1.

Synthesis of $[Pr_3(OtBu)_9(HOtBu)_2]$ (1). HO*t*Bu (in excess, 20 mL) was added to a solution of $[Pr\{N(SiMe_3)_2\}_3]$ (4.2 g, 6.7 mmol) in hexane (25 mL) and THF (5 mL). Herein, a liquid nitrogen bath was used for cooling to avoid a too vigorous reaction. The reaction mixture was stirred at room temperature for 24 h. Recrystallization from a toluene solution (15 mL) followed by cooling at 4 °C produced

DOI: 10.1021/acs.inorgchem.5b00529
Inorg. Chem. 2015, 54, 6267−6280

Table 2. Solutions (Activation Agents) Used for the Activation of the Precursor Solutions Prior to Solvothermal Treatment

activation agent	description	concn	pH	volume added	precursor
KOH_{aq}	aqueous potassium hydroxide solution	$c(KOH)$ = 1.87 mol/L, $c(OH^-)$ = 1.87 M	14 (calcd pH 14.27)	1 mL	**1**, **2**
KOH_{aq}/HO*i*Pr	1 mL of KOH_{aq} diluted in 20 mL of HO*i*Pr	$c(OH^-)$ = 0.09 M	9	20 mL	**1**, **2**
NH_4OH_{aq}	aqueous ammonium hydroxide solution	$c(NH_4OH)$ = 18−30 wt %	14 (calcd pH 14.87)	1 mL	**1**, **2**
H_2O	water diluted in 10 mL of HO*i*Pr or hexane	$c(H_2O)$ = 1 or 5 molar equiv	7	10 mL of HO*i*Pr or hexane + 1 or 5 molar equiv of H_2O	**1**, **2**, **4**

light green crystals of **1**. Yield: 96%, 2.6 g. Anal. Calcd for $[Pr_3(OtBu)_9(HOtBu)_2]$: C, 43.0; H, 8.3. Found: C, 42.2; H, 8.2.

Synthesis of $HOCtBu_3$ (H-tritox). Synthesis of H-tritox was performed following a procedure described in the literature.[22] A solution of diethyl carbonate (6.18 mL, Sigma-Aldrich, puriss, >99.5%) in diethyl ether (50 mL) was slowly (2 h) added to a solution of *tert*-butyllithium (90 mL, 1.7 M in pentane, Acros Organics) and stirred at room temperature. For the hydroxylation of residual *tert*-buthyllithium, a mixture of water (50 mL) and acetic acid (10 mL) was added (T = 0 °C). The compound was isolated by washing with diethyl ether under addition of sodium hydrogen carbonate. After drying with magnesium sulfate, the product was obtained from the organic phase as a waxy solid that could be purified by sublimation at 80 °C ($p \approx 10^{-3}$ mbar). Yield: 60%, 6.1 g. ^{1}H NMR (hexadeuteriobenzene, C_6D_6): δ (ppm) 1.22 (s, 27 H, $-C(CH_3)_3$). ^{13}C NMR (C_6D_6): δ (ppm) 84.53 (s, 1 C, −COH), 44.43 (s, 3 C, $-C(CH_3)_3$), 32.00 (s, 9 C, $-C(CH_3)_3$).

Synthesis of [Pr(tritox)$_3$(THF)] (2). A solution of H-tritox in hexane (2.6 g, 13.1 mmol in 20 mL) was dropped into a solution of $[Pr\{N(SiMe_3)_2\}_3]$ in hexane (2.7 g, 4.4 mmol in 50 mL) and stirred at room temperature for 24 h. After removal of the solvent, the obtained compound was redissolved in a hexane/THF mixture (5 mL/2 mL) and cooled to 4 °C. Light green crystals were obtained that could be identified as $[Pr\{OC(tBu)_3\}_3(THF)]$. Yield: 90%, 3.2 g. Anal. Calcd for $[Pr(tritox)_3(THF)]$: C, 63.7; H, 11.1. Found: C, 63.3; H, 11.2.

Synthesis of $[PrCl\{N(SiMe_3)_2\}_2(THF)]_2$ (3). A solution of $[Pr\{N(SiMe_3)_2\}_3]$ (1.3 g, 2.1 mmol) in toluene (25 mL) was slowly dropped into a suspension of $PrCl_3$ (0.3 g, 1.03 mmol) activated with THF (5 mL) with cooling of the reaction with liquid nitrogen. The reaction mixture was stirred at room temperature for 18 h. Condensation and resolution in hexane and THF followed by cooling at 4 °C produced light green crystals of **3**. Yield: 55%, 0.97 g. Anal. Calcd for $[PrCl\{N(SiMe_3)_2\}_2(THF)]_2$: C, 33.8; H, 7.8; N, 4.9. Found: C, 32.8; H, 7.7; N, 4.7.

Synthesis of $[PrCl\{tritox\}_2(THF)]_2$ (4). Compound **4** was synthesized by dropping a solution of H-tritox (0.4 g, 2.1 mmol) in hexane (25 mL) into a solution of $[PrCl\{N(SiMe_3)_2\}_2]$ (0.5 g, 1.03 mmol) in hexane (25 mL), followed by stirring for 14 h at room temperature. Light green crystals of **4** were obtained from a concentrated solution in a hexane/THF mixture kept at 4 °C. Yield: 72%, 0.92 g. Anal. Calcd for $[PrCl\{tritox\}_2(THF)]_2$: C, 55.7; H, 9.7. Found: C, 54.6; H, 9.6.

Single-Crystal X-ray Diffraction Analysis. Molecular structures of compounds **1**−**4** were determined by single-crystal X-ray diffraction analysis using a diffractometer AED 2 by Siemens. The molecular structures were solved using the software SHELXS-86 and SHELXS-93. All crystallographic data and structure refinement results for compounds **1**−**4** are summarized in Table 1 (absorption correction, numerical; refinement method, full-matrix least-squares on F^2). The Cambridge Crystallographic Data Centre (CCDC) contains the supplementary crystallographic data for this paper. These data can be obtained free of charge from the CCDC via www.ccdc.cam.ac.uk.

Materials Synthesis and Characterization. For solvothermal synthesis, 200 mg of the precursor (**1**, **2**, or **4**) was dissolved in isopropyl alcohol (20 mL) followed by the addition of an activation agent to initialize the hydrolysis of the precursor molecules ("activation"). To study the influence of the nature of the activation agent (pH, concentration) on the material formation, three different basic solutions as well as stoichiometric amounts of water were added. Table 2 summarizes all applied activation agents.

In a first approach, the prepared precursor solutions (precursor **1** or **2**) were activated by addition of an aqueous potassium hydroxide solution (1 mL of KOH_{aq}). Furthermore, precursor solutions of **1** or **2** were also activated by adding 20 mL of a diluted aqueous potassium hydroxide solution (KOH_{aq}/HO*i*Pr). Alternatively, an aqueous solution of ammonium hydroxide (1 mL of NH_4OH_{aq}) was used for the activation of **1** or **2** prior to the solvothermal treatment. Besides activation with a basic activation agent, **1**, **2**, or **4** (ca. 200 mg) in isopropyl alcohol (25 mL) was activated by adding a stoichiometric amount of water (1 or 5 molar equiv in 10 mL of isopropyl alcohol). Finally, the solvothermal decomposition of **1**, **2**, and **4** (ca. 200 mg) was also examined in hexane (25 mL) as a nonpolar solvent following the addition of either 1 mL of KOH_{aq} (precursor **1** and **2**) or a stoichiometric amount of water (1 or 5 molar equiv in 10 mL of hexane, precursors **1**, **2**, and **4**).

The activated solutions were introduced under ambient conditions in Teflon liners, which were enclosed in steel autoclaves (DAB-2, Berghof Products + Instruments GmbH) and heated to 200 °C or 250 °C for 24 h. After cooling to room temperature, the precipitates were washed once with methanol (20 mL) and twice with ethanol (20 mL), collected by centrifugation, dried in air, and ground with a mortar and pestle before further characterization. A summary of all synthesis parameters is given in Table 3. The crystallinity and phase composition of the obtained powders were determined by powder X-ray diffraction analysis at room temperature on a D-5000 Siemens (40 kV, 25 mA, step width 0.02°) or a PW 1710 Philips (45 kV, 30 mA, step width 0.02°) diffractometer operating with Cu Kα_1 radiation. Phase assignment was affected using the program X'Pert HighScore by Philips Analytical B.V. (Almelo, The Netherlands). Transmission electron microscopy (TEM) images of the nanostructures dispersed in isopropyl alcohol and subsequently transferred to a carbon film supported copper grid were obtained with a JEOL 200 CX (Philips) transmission electron microscope. Investigation of the silicon content in the obtained powders was done with the aid of X-ray photoelectron spectroscopy (XPS) using a Surface Science Instrument M-Probe at room temperature (U = 10 keV, I = 15 mA).

RESULTS AND DISCUSSION

Precursor Synthesis and Crystal Structures. Praseodymium *tert*-butoxide $[Pr_3(OtBu)_9(HOtBu)_2]$ (**1**) was obtained by room temperature alcoholysis of $[Pr\{N(SiMe_3)_2\}_3]$ with an excess of *tert*-butyl alcohol. Light green, moisture- and air-sensitive crystals grown from a concentrated solution in toluene at 4 °C revealed a trigonal arrangement of praseodymium atoms (Figure 1) supported by three doubly bridging alkoxy ligands present along the sides of the hypothetical triangle (O3, O4, and O5). Two additional μ_3-bridging alkoxy ligands (O1 and O2) are present below and above the triangular plane, resulting in a 6-fold oxygen coordination around each of the Pr centers as generally favored by this class of lanthanide compounds.[12,23] The obtained molecular structure is similar to those reported for yttrium, lanthanum, terbium, and gadolinium *tert*-butoxides.[6a,b,11,13] Herein, the Pr−O bond lengths (Table 4) fit well with the trend of the Ln−O bond

DOI: 10.1021/acs.inorgchem.5b00529
Inorg. Chem. 2015, 54, 6267−6280

Table 3. Overview of Parameters Used in the Solvothermal Process

key param	precursor[a]	solvent	activation agent
precursor chemistry[b]	**1**	20 mL of HO*i*Pr	KOH_{aq}
	2	20 mL of HO*i*Pr	KOH_{aq}
basic activation[b]	**1**	20 mL of HO*i*Pr	HO*i*Pr/KOH_{aq}
	1	20 mL of HO*i*Pr	NH_4OH_{aq}
	2	20 mL of HO*i*Pr	HO*i*Pr/KOH_{aq}
	2	20 mL of HO*i*Pr	NH_4OH_{aq}
activation by H_2O[c]	**1**	25 mL of HO*i*Pr	1 molar equiv of H_2O in 10 mL of HO*i*Pr
	1	25 mL of HO*i*Pr	5 molar equiv of H_2O in 10 mL HO*i*Pr
	2	25 mL of HO*i*Pr	1 molar equiv of H_2O in 10 mL of HO*i*Pr
	2	25 mL of HO*i*Pr	5 molar equiv of H_2O in 10 mL HO*i*Pr
	4	25 mL of HO*i*Pr	1 molar equiv of H_2O in 10 mL of HO*i*Pr
	4	25 mL of HO*i*Pr	5 molar equiv of H_2O in 10 mL of HO*i*Pr
solvent[c]	**1**	25 mL of hexane	KOH_{aq}
	2	25 mL of hexane	KOH_{aq}
	1	25 mL of hexane	1 molar equiv of H_2O in 10 mL of hexane
	1	25 mL of hexane	5 molar equiv of H_2O in 10 mL of hexane
	2	25 mL of hexane	1 molar equiv of H_2O in 10 mL of hexane
	2	25 mL of hexane	5 molar equiv of H_2O in 10 mL of hexane
	4	25 mL of hexane	1 molar equiv of H_2O in 10 mL of hexane
	4	25 mL of hexane	5 molar equiv of H_2O in 10 mL of hexane

[a]Precursor amount 200 mg. [b]Temperature 200 °C, reaction time 24 h. [c]Temperature 250 °C, reaction time 24 h.

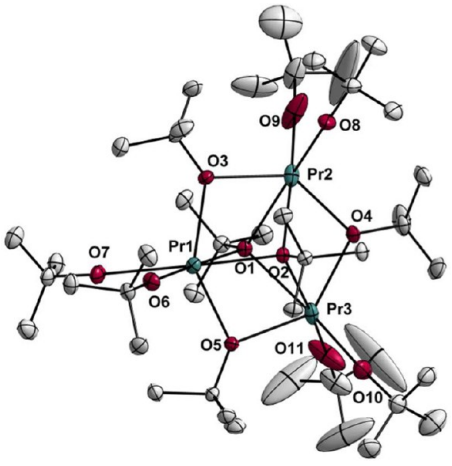

Figure 1. Molecular structure of $[Pr_3(OtBu)_9(HOtBu)_2]$ (**1**). The hydrogen atoms were omitted for clarity.

lengths within the lanthanide series, exhibiting shorter bond lengths with increasing atomic number (selected bond lengths

Table 4. Selected Bond Lengths and Angles in 1

moiety	length (Å)	moiety	angle (deg)
Pr1–O1	2.4890(18)	O3–Pr1–O5	143.11(6)
Pr1–O2	2.4721(17)	O1–Pr1–O2	66.71(6)
Pr1–O3	2.3942(19)	O6–Pr1–O7	72.18(7)
Pr1–O5	2.4137(18)	O3–Pr2–O4	138.11(6)
Pr1–O6	2.1912(18)	O1–Pr2–O2	63.76(5)
Pr1–O7	2.6639(19)	O8–Pr2–O9	86.20(11)
Pr2–O3	2.4702(19)	O4–Pr3–O5	138.05
Pr2–O4	2.4340(19)	O1–Pr3–O2	63.69(5)
Pr3–O4	2.4314(19)	O10–Pr3–O11	86.32(13)
Pr3–O5	2.4417(18)	Pr1–O3–Pr2	98.97(6)
		Pr2–O4–Pr3	102.04(6)
		Pr3–O5–Pr1	99.63(7)

between Ln and μ_3-bridging O: La, 2.505 (13) Å;[10] Pr, 2.4721(17) Å; Nd, 2.409 (13) Å;[12] Gd, 2.3610 (15) Å;[6a] Tb, 2.343(3) Å;[6b] Er, 2.305(3) Å[24]) (selected bond lengths between Ln and μ_2-bridging O: La, 2.449(14) Å;[10] Pr, 2.4137(18) Å; Nd, 2.399(3) Å;[12] Gd, 2.3313(16) Å;[6a] Tb, 2.320(4) Å;[6b] Er, 2.269(3) Å[24]) (selected bond lengths between Ln and terminal alkoxy as well as *tert*-butyl alcohol (with the exception of the Nd complex where THF was reported as a molecule ligate) ligands: La, 2.195(13) Å/2.604(15) Å;[10] Pr, 2.1912(18) Å/2.6639(19) Å; Nd, 2.147(4) Å/2.661(4) Å;[12] Gd, 2.1223(16) Å/2.5567(16) Å;[6a] Tb, 2.114(4) Å/2.609(4) Å;[6b] Er, 2.067(3) Å/2.525(4) Å[24]). Despite its discrete molecular structure, **1** cannot be vaporized due to coordinated alcohol ligands that are removed under vacuum, thus producing higher agglomerates with evidently low vapor pressure. One of the praseodymium atoms (Pr1) is coordinated by two alkoxy groups, whereas two other praseodymium atoms (Pr2 and Pr3) bear one alkoxy ligand and one *tert*-butyl alcohol each. Consequently, bond angles (Table 4) around Pr1 (Figure 1), (O3–Pr1–O5, 143.11(6)°; O6–Pr1–O7, 72.18(7)°) are significantly different from analogous bond angles of Pr2 (O3–Pr2–O4, 138.11(6)°; O8–Pr2–O9, 86.20(11)°) and Pr3 (O4–Pr3–O5, 138.05(6)°; O10–Pr3–O11, 86.32(13)°).

The observed trinuclear structural motif has been frequently observed in various homoleptic and heteroleptic derivatives of yttrium and lanthanide elements.[6a,b,11,13,25] This arrangement is apparently favored due to the tendency of trivalent lanthanide ions to expand their coordination number, as this specific ligand-deficit arrangement allows 6-fold coordination of oxygen atoms around each of the metal centers. The large body of data available on metal alkoxides suggests that the synthesis of complexes with lower nuclearity would require bulkier ligands capable of providing an optimal steric shielding of the lanthanide centers.[26] In the case of smaller ligands, the coordination of solvent molecules as neutral ligands is generally observed to achieve a preferable coordination state for the central metal atom. Alternatively, polydentate ligands are useful for controlling the nuclearity of molecules via steric hindrance and saturation of available coordination sites.[9,27]

To investigate the influence of the precursor's molecular structure on its decomposition behavior and eventual formation of praseodymium-based nanostructures, we aimed for the synthesis of monomeric praseodymium alkoxide. Therefore, the bulky tris-*tert*-butoxide (tritox) ligand was chosen to modify $[Pr\{N(SiMe_3)_2\}_3]$ with 3 equiv of $HOCtBu_3$ to produce $[Pr\{OC(tBu)_3\}_3(THF)]$ (**2**):

DOI: 10.1021/acs.inorgchem.5b00529
Inorg. Chem. 2015, 54, 6267–6280

$$[Pr\{N(SiMe_3)_2\}_3] + 3HOC(tBu)_3 \xrightarrow[-3HN(SiMe_3)_2]{\text{hexane, THF}} \underset{\mathbf{2}}{[Pr\{OC(tBu)_3\}_3(THF)]} \quad (1)$$

Compound **2** crystallized in the triclinic space group $P\bar{1}$ (Figure 2), whereby the lower symmetry of the crystal structure

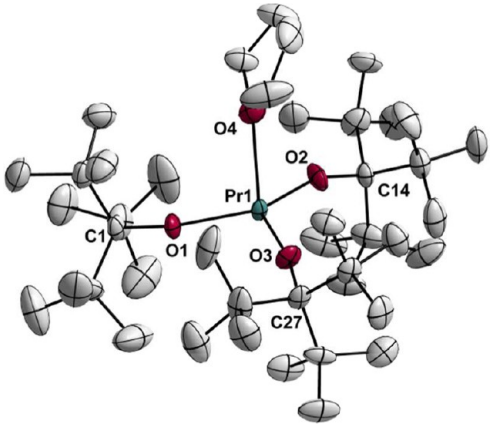

Figure 2. Molecular structure of $[Pr\{OC(tBu)_3\}_3(THF)]$ (**2**). The hydrogen atoms were omitted for clarity.

resulted from the bulky ligands not allowing a denser packing of the structural units. As a result, **2** displayed a 4-fold oxygen environment with pseudotetrahedral coordination bestowed by a donor THF molecule. As expected, the bond length (Table 5)

Table 5. Selected Bond Lengths and Angles in 2

moiety	length (Å)	moiety	angle (deg)
Pr1–O1	2.196(6)	O1–Pr1–O2	114.6(22)
Pr1–O2	2.172(6)	O2–Pr1–O3	122.5(2)
Pr1–O3	2.186(6)	O3–Pr1–O1	117.9(2)
Pr1–O4	2.524(7)	O4–Pr1–O1	103.5(2)
O1–C1	1.414(10)	O4–Pr1–O2	89.3(2)
		O4–Pr1–O3	99.9(2)

between the central praseodymium atom and the THF ligand (Pr1–O4, 2.524(7) Å) was significantly longer when compared to Pr–tritox bond lengths (average bond length 2.185(3) Å). Furthermore, the strong steric repulsion among the tritox periphery caused a broadening of the bond angles among the tritox ligands when compared to those of *tert*-butoxide derivatives.[6b] As described for the analogous terbium tris-*tert*-butoxide derivative,[6b] Pr–O bond lengths in the mononuclear **2** (average bond length 2.185(3) Å) are shorter than those in trinuclear **1** (average bond length 2.447(2) Å). Besides terbium and praseodymium tritox derivatives, neodymium and cerium tritox compounds have been reported by Wedler et al.[28] and Stecher et al.,[29] respectively. The synthesis of single crystals in the case of neodymium as the metal ion has been reported, revealing the formation of the monomeric crystal structure $[Nd\{OC(tBu)_3\}_3(THF)]$ by X-ray analysis; however, the bond lengths and angles were not discussed.[28] The formation of solvent-free $[Nd\{OC(tBu)_3\}_3]$ crystals was reported by Herrmann et al., yet single-crystal X-ray diffraction analysis on the obtained crystals could not be provided.[30] Furthermore, the crystallization of the tris-*tert*-butoxide derivative of ytterbium has been reported.[31] $[Yb\{OC(tBu)_3\}_2(THF)_2]$ exhibits only two tritox ligands, while the pseudotetrahedral coordination is completed by the coordination of two THF molecules. With respect to analogous lanthanide tritox complexes, the obtained bond lengths in **2** follow the trend of decreasing bond lengths with increasing atomic number from praseodymium (average Pr–tritox bond length, 2.185 Å; Pr–THF bond length, 2.524(7) Å) to terbium[6b] (average Tb–tritox bond length, 2.113 Å; Tb–THF bond length, 2.401(5) Å) and erbium (average Er–tritox bond length, 2.077 Å; Er–THF bond length, 2.335(7) Å (unpublished data)).

The reaction of 2 equiv of $[Pr\{N(SiMe_3)_2\}_3]$ with 1 equiv of $PrCl_3$ resulted in a ligand-scrambling reaction to produce the heteroleptic species $[PrCl\{N(SiMe_3)_2\}_2(THF)]_2$ (**3**), which acted as a synthon to $[PrCl\{OC(tBu)_3\}_2(THF)]_2$ (**4**) by replacing the amide ligands with tritox units:

$$\underset{\mathbf{3}}{[PrCl\{N(SiMe_3)_2\}_2]_2} + 4HOC(tBu)_3 \xrightarrow[-4HN(SiMe_3)_2]{\text{hexane, THF}} \underset{\mathbf{4}}{PrCl\{OC(tBu)_3\}_2(THF)]_2} \quad (2)$$

Compounds **3** and **4** were obtained as light green needles from a mixture of hexane and THF maintained at 4 °C. Single-crystal X-ray diffraction structure analysis of **3** (monoclinic, space group $P2_1/n$) revealed a centrosymmetric, chloro-bridged dinuclear molecular structure (Figure 3). Additional coordina-

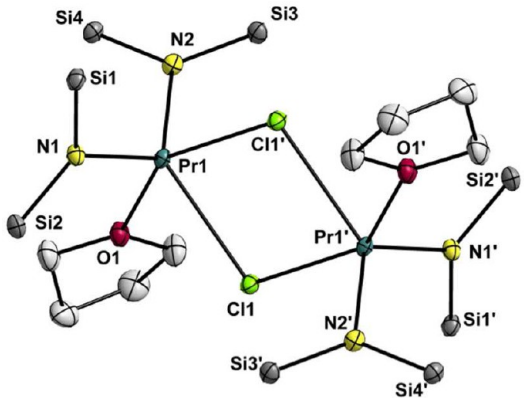

Figure 3. Molecular structure of $[PrCl\{N(SiMe_3)_2\}_2(THF)]_2$ (**3**). The hydrogen and carbon atoms of the amide groups were omitted for clarity.

tion of one THF molecule at each coordination center compensates for the lack of electrons at the praseodymium centers. Analogous molecular structures for stable bisamido chloride complexes of the type $[Ln\{N(SiMe_3)_2\}_2(THF)(\mu\text{-}Cl)]_2$ have been reported by Karl et al. for samarium and by Berg et al. for neodymium obtained through the reaction between the lanthanide amide $Ln[N(SiMe_3)_2]_3$ and the lanthanide chloride $LnCl_3$ (Ln = Sm, Nd).[32] In contrast, the analogous europium complex was found not to be stable.[33] In a similar approach, the reaction between sodium or lithium amide with the lanthanide chloride was reported to yield isostructural crystals of ytterbium, gadolinium, neodymium, and cerium bisamido chloride.[32b,33b,34] Within this set of reported lanthanide bisamido chloride complexes, the determined bond lengths (Table 6) in the here discussed praseodymium complex follow the decreasing trend toward ytterbium (average Ln–Cl bond lengths: Pr, 2.828 Å; Nd, 2.823 Å;[32b] Sm, 2.782 Å;[32a] Gd, 2.753 Å;[33b] Yb, 2.679 Å[33b]) (average Ln–N bond lengths: Pr, 2.306 Å; Nd, 2.318 Å;[32b] Sm, 2.272 Å;[32a] Gd, 2.252 Å;[33b] Yb,

DOI: 10.1021/acs.inorgchem.5b00529
Inorg. Chem. 2015, 54, 6267–6280

Table 6. Selected Bond Lengths and Angles in 3

moiety	length (Å)	moiety	angle (deg)
Pr1−Cl1	2.8284(3)	Cl1#1−Pr1−Cl1	74.002(9)
Pr1−N1	2.2996(10)	Cl1−Pr1−O1	77.99(2)
Pr1−N2	2.3130(10)	O1−Pr1−N2	85.21(3)
Pr1−O1	2.5433(9)	N2−Pr1−Cl1#1	99.67(3)
		N1−Pr1−Cl1#1	93.57(3)
		N1−Pr1−Cl1	111.02(3)
		N1−Pr1−O1	111.30(3)
		N1−Pr1−N2	120.89(4)

2.186 Å[33b]) (Ln−O bond lengths: Pr, 2.5433(9) Å; Nd, 2.496(7) Å;[32b] Sm, 2.469(8) Å;[32a] Gd, 2.444(5) Å;[33b] Yb, 2.351(5) Å[33b]).

The molecular structure of **4** is isostructural with that of compound **3** (Figure 4); however, the introduction of the

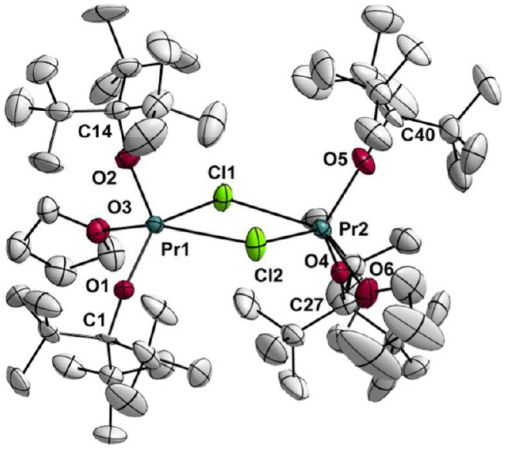

Figure 4. Molecular structure of $[PrCl\{OC(tBu)_3\}_2(THF)]_2$ (**4**). The hydrogen atoms were omitted for clarity.

bulkier tritox ligands resulted in a hindered packing of the structural units and therefore in a reduced crystal symmetry (space group $P\bar{1}$). With a value of 2.8284(3) Å, the Pr−Cl bond length (Table 7) in **3** is longer than the Pr−N bond length

Table 7. Selected Bond Lengths and Angles in 4

moiety	length (Å)	moiety	angle (deg)
Pr1−Cl1	2.909(3)	Cl1−Pr1−Cl2	73.46(10)
Pr1−O1	2.099(7)	Cl2−Pr1−O1	94.7(2)
Pr1−O2	2.114(6)	O1−Pr1−O3	93.5(3)
Pr1−O3	2.586(8)	O3−Pr1−Cl1	76.29(18)
		O2−Pr1−Cl1	109.9(2)
		O2−Pr1−Cl2	108.9(2)
		O2−Pr1−O1	111.0(3)
		O2−Pr1−O3	102.3(3)

(2.2996(10) and 2.3130(10) Å), indicating its higher ionic nature. The Pr−O bond lengths (**4**: Pr1−O1, 2.099(7) Å; Pr1−O2, 2.114(6) Å) are shorter than the Pr−N bond lengths (**3**: Pr1−N1, 2.2996(10) Å; Pr1−N2, 2.3130(10) Å) due to the higher basicity of oxygen atoms. The bond lengths as well as angles in **4** are in agreement with those of the analogous neodymium compound obtained by the reaction of $[NdCl_3(THF)_2]$ with $Li(OCtBu_3)$ described by Wedler et al.[28] In both compounds, coordination of additional THF molecules at the Ln centers resulted in a distorted trigonal bipyramidal geometry around the metal center. However, the preferred octahedral coordination could not be achieved due to steric constraints. The molecular structure of **4** is formed by two tritox ligands (O1, O2) and one chloro ligand (Cl1) arranged in the equatorial plane around the praseodymium center (O1−Pr1−O2, 111.0(3)°; O1−Pr1−Cl1, 139.04(18)°; O2−Pr1−Cl1, 109.9(2)°), while the second chloro ligand (Cl2) and a THF molecule (O3) are located below and above the triangular plane (O3−Pr1−Cl2, 142.18(17)°). The coordination figure is similar to that observed in **3**, where one chloro ligand (Cl1) and two bis((trimethylsilyl)amido) ligands (N1, N2) (N1−Pr1−Cl1, 111.02(3)°; N1−Pr1−N2, 120.89(4)°; N2−Pr1−Cl1, 128.04(3)°) form the equatorial plane, while ligands O1 and Cl1#1 are located above and below this plane (O1−Pr1−Cl1#1, 147.78(2)°).

Further Analysis of 1−4. Aiming for a characterization of the synthesized compounds in solution, NMR measurements were carried out, yet due to the paramagnetism of praseodymium, the obtained data were not conclusive. Furthermore, UV−vis spectra recorded on solutions of **1**−**4** did not provide any significant features in the visible range, which can be expected taking into account that the f−f transitions in praseodymium are forbidden. However, elemental analysis data found for compounds **1**−**4** are in good agreement with the calculated content of C, H, and N. For the alkoxides **1**, **2**, and **4**, the found concentrations in C and H differ by less than 2% from the calculated concentrations. For amido compound **3**, a maximal deviation of 4% was found in the case of N (calculated, 4.9%; found, 4.7%). Deviations between calculated and found concentrations can be explained by partial decomposition of the highly air- and moisture-sensitive compounds during handling and transfer to the CHN analyzer. Thus, these data provide further evidence for the suggested identity of the synthesized compounds in the form of bulk powder.

TG/DTA Analysis. TG/DTA profiles recorded for precursors **1**−**4** (Figure 5) revealed the influence of the chosen ligand on the decomposition mechanism. **1** showed a total mass loss of 69% in three steps at 204, 277, and 328 °C (Figure 5a), which were accompanied by endothermal peaks in the corresponding DTA curve possibly due to ligand elimination and fragmentation. The mass loss of 12% found at a temperature of 200 °C can be assigned to the loss of the two coordinated *tert*-butyl alcohol molecules (found residual mass, 1081.5 g/mol; theoretical mass of $Pr_3(OtBu)_9$, 1081.0 g/mol). Further elimination of organic ligands is evident as a second mass loss of 32% in the temperature range of 255−305 °C and a third mass loss of 24% at a temperature of 330 °C. Formally, these second and third mass losses together could be assigned to the elimination of the residual *tert*-butyl groups (second step, found mass loss 32% or 393 g/mol, corresponding to 5.4 O*t*Bu groups; third step, found mass loss 24% or 295 g/mol, corresponding to 4.0 O*t*Bu groups). The resulting residual mass of 31% may formally be assigned to praseodymium carbonate phase $Pr_2O_2CO_3$ (found residual mass, 31% or 381 g/mol; theoretical residual mass for $Pr_2O_2CO_3$, 30.4% or 373.8 g/mol). As the TG/DTA analysis was performed under inert conditions, compound **1** itself must be considered as a carbon source,[30] inducing the formation of the carbonate phase. As described in the section "Materials Synthesis", the formation of $Pr_2O_2CO_3$ was in fact observed as a crystalline phase after the solvothermal treatment of **1** following activation with a stoichiometric amount of water (Figure 11).

DOI: 10.1021/acs.inorgchem.5b00529
Inorg. Chem. 2015, 54, 6267−6280

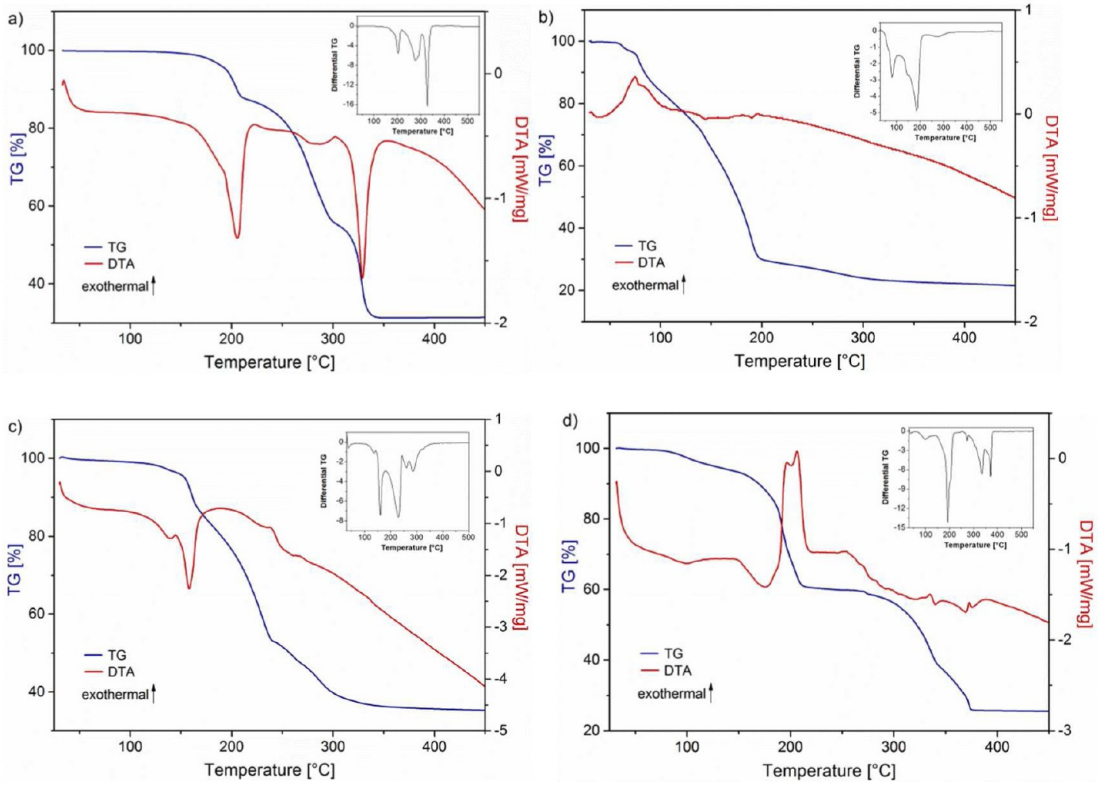

Figure 5. TG/DTA analysis of (a) **1**, (b) **2**, (c) **3**, and (d) **4**.

Compound **2** (Figure 5b) also showed a decomposition profile in three steps (as apparent from the differential TG graph, inset of Figure 5b). However, all peaks are less pronounced and shifted to lower temperatures when compared to those of **1**, suggesting a different chemical influence when both compounds are used as precursor molecules in materials synthesis. In the low temperature range, volatile components or the coordinated THF molecule is eliminated (found mass loss until 83 °C, 9.3%; found residual mass, 735 g/mol; theoretical mass loss for the elimination of one THF, 8.8%; theoretical residual mass, 739 g/mol), while the main mass loss (60%) due to the elimination of organic groups is observed in the temperature range of 83−200 °C. The final mass loss occurs at temperatures above 200 °C. Hermann et al. identified mass spectroscopic fragments of $(tC_4H_9)_2CO$ and H-tritox, respectively H-ditox, during the thermal decomposition of $Nd(tritox)_3$ until 330 °C.[30] The residual mass of 20% (~162 g/mol) can formally be assigned to the formation of praseodymium oxide $PrO_{1.83}$, which has also been found upon annealing in air of solvothermally obtained $Pr(OH)_3$ powders (found residual mass, 20% or 162 g/mol; theoretical residual mass in the case of $PrO_{1.83}$, 21% or 170 g/mol).

Thermal decomposition of heteroleptic compounds **3** and **4** occurred in multiple steps (five steps are indicated by the differential TG curves, insets in Figure 5c,d). The endothermal feature observed at 158 °C in the case of **3** corresponds to a mass loss of 11.4% and is due to the removal of a coordinated THF molecule (theoretical mass loss 12.7%); the elimination of amide ligands most likely caused the two-step mass loss of 35% and 17% in the temperature range of 165−360 °C (found residual mass: first step, 307 g/mol; second step, 208 g/mol) (theoretical residual mass: after elimination of one amide group, 337 g/mol; after elimination of two amide groups, 176 g/mol). The residual mass of 35% (199 g/mol) indicated the formation of PrOCl (theoretical residual mass 192.4 g/mol or 34%) at the end of the decomposition process. Introduction of the tritox ligand in **4** resulted in two main differences in the TG/DTA curves when compared to those of **3** (Figure 5d). First, the first endothermal feature is detected at a temperature below 100 °C, indicating a lower initial decomposition temperature of **4** when compared to **3**. Second, a prominent exothermal peak was detected at 206 °C that can be due to combustion of organic groups and the beginning of incipient crystallization processes. The TG curve reveals one main step in this temperature range followed by a second mass loss, both assigned to the elimination and fragmentation of the tritox ligands (theoretical residual mass loss after removal of one tritox, 394 g/mol; found residual mass loss at 215 °C, 405 g/mol; theoretical residual mass loss after removal of two tritox molecules, 194 g/mol; found residual mass loss at 378 °C, 173 g/mol). Formally, the found residual mass of 25% (166 g/mol) may indicate the formation of PrOCl as already seen in the case of **3** (theoretical residual mass in the case of formation of PrOCl from **4**, 29%). As in the case of **1**, the TG/DTA data of **4** give evidence for the formation of a crystalline phase, namely, PrOCl, that corresponds to the crystalline phase that also has been observed in powders obtained by solvothermal treatment. The formation of PrOCl upon solvothermal treatment of **4** after activation with a stoichiometric amount of water is described in the following section (Figure 11).

The interplay of the coordination number and nature of the ligands is evident in the observed molecular structures of compounds **1**−**4**. The nuclearity of the complex increased with increasing coordination number from mononuclear (**2**) to binuclear (**3**, **4**) to finally trinuclear (**1**). Accordingly, on the basis of the differential TG (insets in Figure 5), the

DOI: 10.1021/acs.inorgchem.5b00529
Inorg. Chem. 2015, 54, 6267−6280

decomposition of the four compounds took place in temperature windows of 35−360 °C (**2**), 65−385 °C (**4**), 100−375 °C (**3**), and 125−360 °C (**1**). Moreover, using the most intense peak of the differential TG (insets in Figure 5) as an indicator, the temperature of the major decomposition step increased from 185 °C (**2**) to 200 °C (**4**), 230 °C (**3**), and 330 °C (**1**).

Materials Synthesis. *Influence of the Precursor Chemistry.* In a first approach for the solvothermal synthesis of nanostructures, a solution of praseodymium precursor **1** or **2** in isopropyl alcohol was mixed to an aqueous potassium hydroxide solution (KOH_{aq}, Table 2) to initiate the precipitation process, followed by an autoclave treatment at 200 °C for 24 h. The solvothermal decomposition of both precursors **1** and **2** led to elongated nanostructures as found in the TEM analysis (Figure 6). The observed morphology and

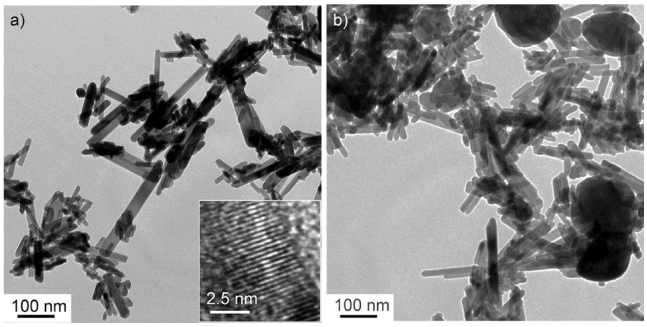

Figure 6. TEM images of powders obtained from (a) **1** and (b) **2** after activation with KOH_{aq} and subsequent solvothermal treatment at 200 °C for t = 24 h.

size distribution were similar to those reported by Ma et al. using microwave-assisted treatment of $Pr(NO_3)_3$ solutions or by hydrothermal treatment of Pr_2O_3 as described by Wang et al.[35] In the case of **2**, particles about 100 nm in diameter were observed together with the rodlike nanostructures. Nanostructures obtained from **1** were shown by X-ray diffraction (XRD) measurements to be single-phase crystalline praseodymium hydroxide, $Pr(OH)_3$ (Figure 7a). Also in the case of **2**, the main crystalline phase was determined to be $Pr(OH)_3$ (Figure 7b). However, a secondary phase was found corresponding to crystalline $Pr_{9.33}Si_6O_{26}$, which possibly formed due to silicon impurities (a residual bis(trimethylsilyl)amide group present in praseodymium silyl amide) originating from precursor synthesis. A similar observation had been reported for a Tb derivative.[6b] The presence of a silica phase in powders obtained from **2**, but not in powders obtained from **1**, was confirmed by XPS (further discussion of the formation of the silicate phase is provided as Supporting Information, Figures S1 and S2).

Lanthanide hydroxides, $Ln(OH)_3$, crystallize in the hexagonal lattice where the anisotropic growth is governed by the crystal chemistry and chemical potential of $Ln(OH)_3$ in solution. Consequently, no templates are required to obtain one-dimensional structures. In agreement with this, nanorods are obtained upon the solvothermal treatment of **1** and **2**. This one-dimensional growth resulting in the formation of nanorods is generally favored by the hexagonal crystal structure of the lanthanide hydroxides, a material intrinsic property. However, as seen in Figure 6, the decomposition of **2** showed a trend for the formation of larger particles as a second morphology. This bimodal morphology observed in powders derived from **2** indicates that there must be further underlying processes governing the materials formation in addition to the intrinsic trend for one-dimensional growth. Such underlying processes may include different nucleation processes active in the hydrolysis and condensation of species formed from **1** and **2** (Scheme 1). On one hand, these processes can support the one-dimensional growth intrinsically triggered by the hexagonal crystal lattice of $Ln(OH)_3$. On the other hand, they could suppress the anisotropic growth as here observed in the case of powders derived from precursor **2**. Generally speaking, the condensation of partially hydrolyzed praseodymium species is triggered by the tendency of praseodymium atoms to achieve higher coordination numbers required for the formation of a thermodynamically favored product.

Thus, the here observed trend for nanorod or particle formation can be explained as follows. In the case of **1**, the higher coordination state (CN = 6) of the praseodymium centers, resulting from the trimetallic Pr_3 unit stabilized by doubly and triply bridging alkoxo groups, together with the higher reactivity of the bridging groups toward a nucleophilic attack (−OH groups) makes the presence of trimetallic hydroxo units in the solution likely. Especially the higher reactivity of the μ_3-bridging groups when compared to the μ_2-bridging groups toward the nucleophilic attack by OH^- must be taken into account. Consequently, the reactivity of the

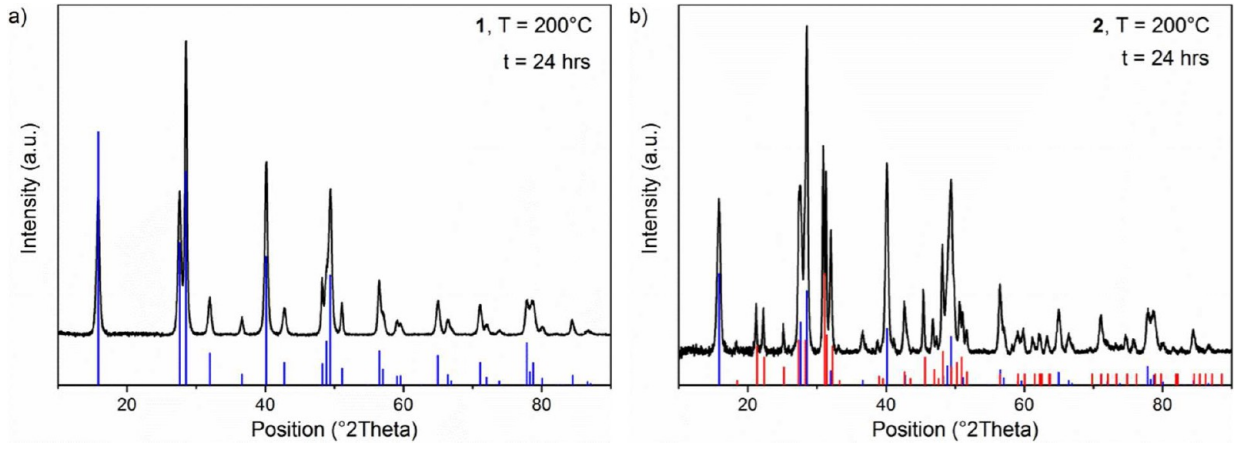

Figure 7. X-ray diffraction patterns of powders obtained by solvothermal treatment (24 h) of (a) **1** and (b) **2** after activation with KOH_{aq}. References: $Pr(OH)_3$, 23-8304 (blue); $Pr_{9.33}Si_6O_{26}$, 23-1389 (red).

DOI: 10.1021/acs.inorgchem.5b00529
Inorg. Chem. 2015, 54, 6267−6280

Scheme 1. Suggested Hydrolysis and Condensation Steps during Solvothermal Treatment of Precursors 1 and 2

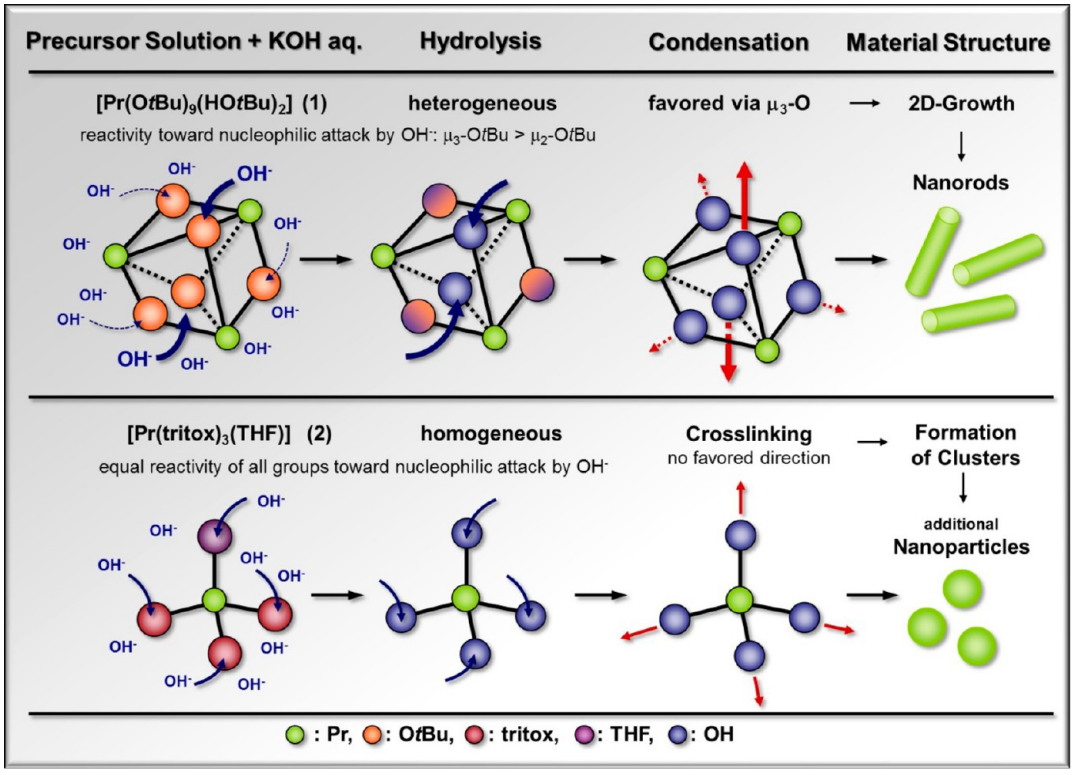

bridging groups is not equally distributed throughout the molecule, but higher reactivity toward hydrolysis and condensation is seen for the μ_3-bridging groups above and below the plane spanned by the three praseodymium atoms. This favored hydrolysis of these μ_3-bridging groups with a subsequently favored condensation via μ_3-O triggers a heterogeneous condensation process and further supports the intrinsic tendency of $Pr(OH)_3$ to form one-dimensional, rodlike structures. In the case of **2**, where all ligands show the same reactivity toward the nucleophilic attack by OH^-, homogeneous hydrolysis of the bulkier tritox ligands would produce coordinatively more unsaturated species due to the lower coordination state of Pr (CN = 4) in the precursor. In addition, the presence of $\{Pr(OH)_4\}^-$ units upon hydrolysis as well as their favored isotropic condensation will promote a quick growth of nuclei, a consumption of smaller particles, and the eventual formation of spherical clusters or particles. Consequently, the intrinsic trend of $Pr(OH)_3$ to form rodlike structures is partially overcome, and clusters and particles are observed besides rodlike structures. These suggested pathways for the hydrolysis and condensation of **1** and **2** are supported by the presence of clusters in the TEM images of products obtained after the solvothermal processing of **2** and the presence of anisotropic nanorods alone in the case of **1**.

Influence of the Precursor Concentration and Nature of the Activation Agent. Control over the shape and aspect ratio was further tuned by variation of the precursor concentration and the activation agent inducing precipitation. While the addition of KOH_{aq} to a solution of **1** or **2** led to strong anisotropic growth (aspect ratio in the range of 5−7.5, Figure 6), the addition of an aqueous ammonium hydroxide solution (NH_4OH_{aq}, Table 2) or the addition of a solution of KOH_{aq} diluted in isopropyl alcohol ($HOiPr/KOH_{aq}$, Table 2) resulted in elongated nanoparticles with significantly lower aspect ratios (in the range of 1−5) (Figure 8). As already observed for powders obtained by solvothermal treatment of **2** after activation with KOH_{aq} (Figure 6b), we here see again a tendency for the formation of irregularly shaped clusters as

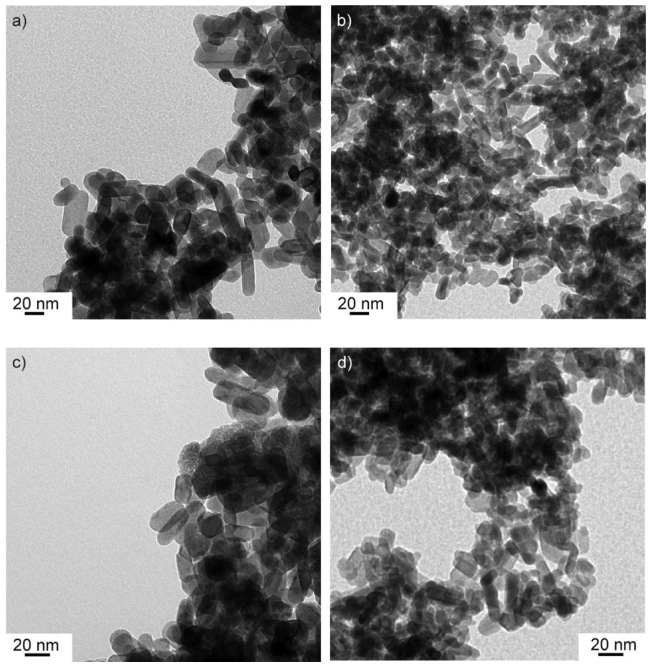

Figure 8. TEM images of powders obtained by solvothermal treatment of **1** after activation with (a) $HOiPr/KOH_{aq}$ and (b) an aqueous solution of NH_4OH_{aq} and analogous powders obtained from **2** after activation with (c) $HOiPr/KOH_{aq}$ as well as (d) NH_4OH_{aq} (T = 200 °C, t = 24 h).

DOI: 10.1021/acs.inorgchem.5b00529
Inorg. Chem. 2015, 54, 6267−6280

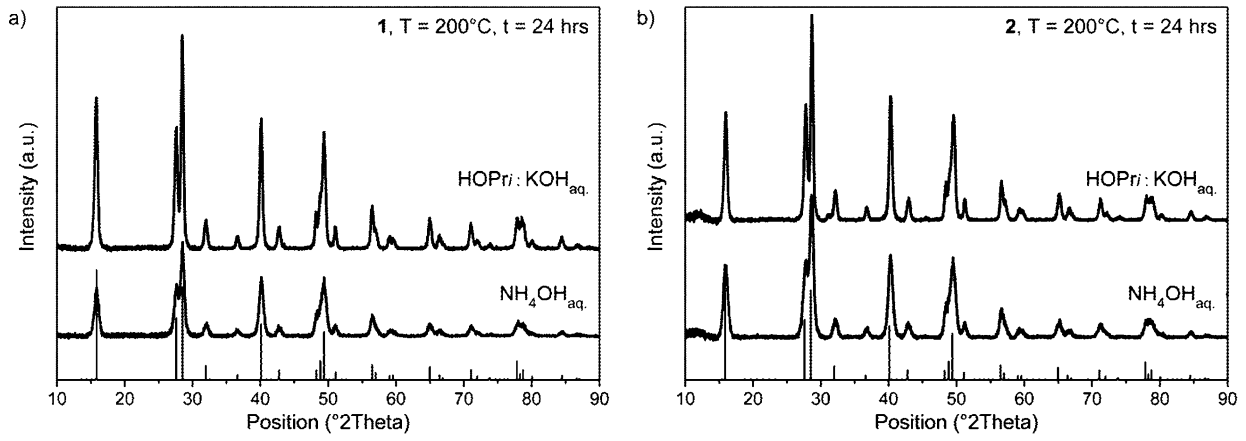

Figure 9. XRD patterns recorded on powders obtained by the solvothermal decomposition of (a) **1** and (b) **2** after activation with either HO*i*Pr/KOH_{aq} or NH_4OH_{aq} (T = 200 °C, t = 24 h). Reference: $Pr(OH)_3$, 23-8304.

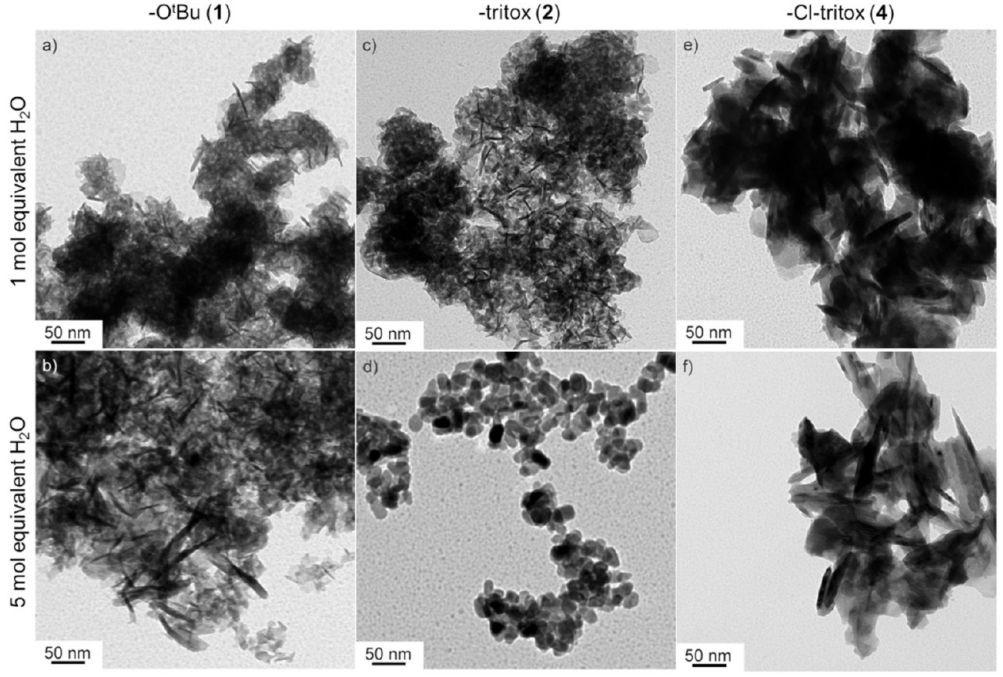

Figure 10. TEM images of powders obtained by solvothermal treatment of **1**, **2**, and **4** after activation with water (T = 250 °C, t = 24 h).

secondary morphology when **2** is activated by addition of HO*i*Pr/KOH_{aq} (Figure 8c). As obvious from the XRD patterns (Figure 9) recorded on the powders, the resultant solid phase consists of pure $Pr(OH)_3$ when **1** and **2** are used as precursors.

Due to the limited volume of the used Teflon liners, the reaction mixture of 20 mL of precursor solution and 20 mL of HO*i*Pr/KOH_{aq} activation agent was portioned to two Teflon liners, which resulted in a halved precursor concentration when compared to that of the previously described case (20 mL of precursor solution and 1 mL of KOH_{aq} additive per Teflon liner). This allows the study of a potential *precursor concentration effect* on the particle size and morphology. In fact, the solvothermal treatment of lower concentrated precursor solutions results in elongated nanoparticles exhibiting a smaller size (ca. 10 nm × 50 nm, Figure 8a; ca. 15 nm × 32 nm, Figure 8c) when compared to those obtained from higher concentrated solutions (Figure 6). This conforms with the observation made by Sohn et al. in the case of precipitation of $Y(OH)CO_3$ from a Y_2O_3 solution under addition of urea.[36] Furthermore, dilution of the precipitation-inducing activation agent not only results in a lower precursor concentration, but also in a lower OH^- concentration ($c(OH^-)_{(KOH_{aq}/HOiPr)}$ = 0.09 M versus $c(OH^-)_{(KOH_{aq})}$ = 1.87 M), and thus in a lower hydrolysis rate and a lower rate of condensation. This led to the precipitation of smaller clusters and finally a reduced particle size after solvothermal treatment. Even smaller nanostructures with a minimal particle size of approximately 30 nm (**1**), respectively 20 nm (**2**), were obtained upon the addition of an aqueous ammonium hydroxide solution (1 mL of NH_4OH_{aq} ($c(OH^-)$ = 7.36 M) added to 20 mL of precursor solution) (Figure 8b,d). As mentioned previously, the 1-dimensional growth of lanthanide hydroxides is favored by the inherent hexagonal crystal lattice and governed by the crystal chemistry and chemical potential of the $Ln(OH)_3$ solution. Generally, a sufficient concentration of OH^- in the reaction mixture results in the formation of $Ln(OH)_3$ nanorods or nanowires. As reported by Li et al. for the formation of $Sm(OH)_3$ and

DOI: 10.1021/acs.inorgchem.5b00529
Inorg. Chem. 2015, 54, 6267−6280

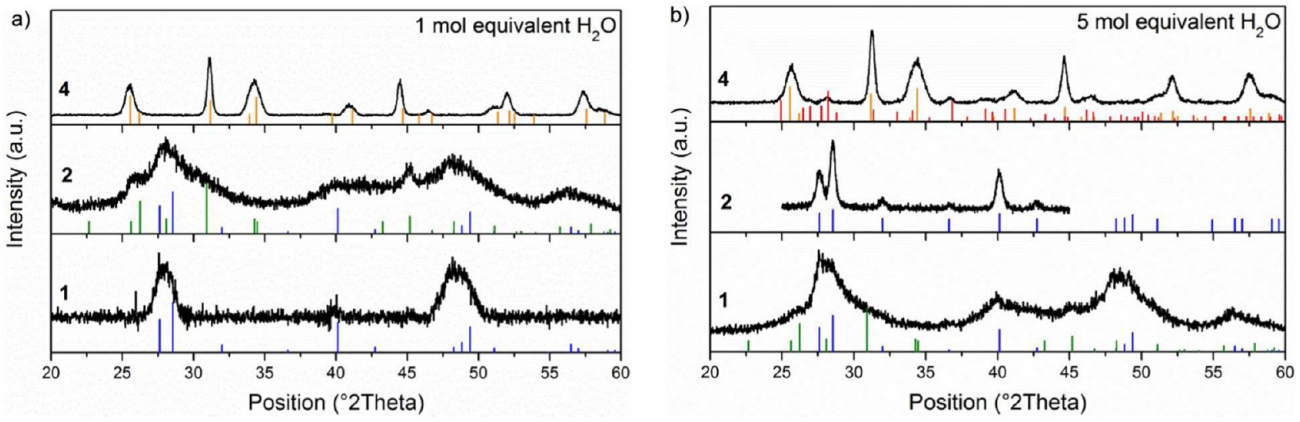

Figure 11. X-ray diffraction patterns of powders obtained by solvothermal treatment (250 °C, 24 h) of **1**, **2**, and **4** after activation with (a) 1 molar equiv and (b) 5 molar equiv of H_2O. References: $Pr(OH)_3$, 23-8304 (blue); $Pr_2O_2CO_3$, 37-0805 (green); PrOCl, 85-0948 (orange); $Pr(OH)_2Cl$, 72-2211 (red).

$Gd(OH)_3$, an increase in pH initially resulted in nanostructures of higher aspect ratio, yet a further increase of the pH induced a drop of the aspect ratio. Consequently, there exists an optimal pH value for the growth of anisotropic nanostructures based on the complex interaction and the OH^- concentration-driven balance between the chemical potential and the rate of ionic motion.[35b,37] Herein, the increased OH^- concentration induces an increased chemical potential in solution, which favors the 1-dimensional growth. A further increase of the OH^- concentration however prominently reduces the concentration of monomer, meaning Ln^{3+}, in the reaction solution, resulting in a smaller diffusion driving force along the axis favored by the hexagonal crystal lattice and consequently in less pronounced 1-dimensional growth, but formation of smaller sized nanoparticles.[37,38] In agreement with this, the formation of nanorods was observed when KOH_{aq} ($c(OH^-)$ = 1.87 M) was used as the activation agent during solvothermal decomposition of **1** and **2**, while KOH_{aq}/HO*i*Pr ($c(OH^-)$ = 0.09 M) produced smaller nanorods of reduced aspect ratio, and NH_4OH_{aq} ($c(OH^-)$ = 7.36 M) resulted in even smaller nanoparticles. This reveals the *importance of pH control* to tune the growth behavior and resultant morphology of $Pr(OH)_3$ nanostructures.

Activation by Addition of Water. We further investigated the relationship between hydrolysis rate, phase, and morphology by adding water instead of bases to isopropanolic solutions of praseodymium compounds **1**, **2**, and **4** prior to the solvothermal treatment at 250 °C for 24 h. Transmission electron micrographs and X-ray diffraction patterns of the obtained powders are given in Figures 10 and 11. All obtained morphologies differ from the characteristic rodlike structure of $Ln(OH)_3$. Nanoparticles 30 nm in diameter are obtained from **2** by addition of 5 molar equiv of water (Figure 10d). Flakelike structures of 50−100 nm edge length were observed in all other cases. Similar structures have been reported for $Y_2O_2CO_3$[39] and $LaOHCO_3$ as well as $CeOHCO_3$.[40] In fact, the expected formation of crystalline $Pr(OH)_3$ was only observed for the addition of 1 molar equiv of water to **1** as well as 5 molar equiv of water to **2** (Figure 11). Hydrolysis of **1** with 5 molar equiv of water, respectively **2** with 1 molar equiv of water, followed by solvothermal treatment led to powders whose X-ray diffraction patterns suggest a phase mixture of partially crystalline $Pr(OH)_3$ and $Pr_2O_2CO_3$ (Figure 11).

The formation of stable carbonate phases could be explained by taking into account the low formation enthalpy of lanthanide carbonates. As shown by Tareen et al., who investigated the formation and stability of carbonate phases in the phase diagrams of Ln_3O_3−H_2O−CO_2 under hydrothermal conditions, $Ln(OH)CO_3$ and $Ln_2O_2CO_3$ of the lighter lanthanides are formed already at low CO_2 concentrations.[41] A potential source of carbon during the solvothermal treatment of **1** and **2** might be found in the precursor molecules themselves upon their decomposition as indicated by TG/DTA analysis. Furthermore, the addition of small but sufficient concentrations of CO_2 from the air during the transfer of the precursor solutions into the Teflon liners cannot be completely ruled out despite precautions being taken such as handling of the liners under a flow of nitrogen. According to Tareen et al., the transition from $Ln(OH)CO_3$ into $Ln_2O_2CO_3$ takes place at 550 °C under hydrothermal conditions,[41] yet the use of an isopropanolic solution instead of pure water for the solvothermal decomposition of **1**, **2**, and **4** led to higher pressure inside the autoclave, which may lower the transition temperature. Veith et al. reported the thermal decomposition of yttrium glycolate into $Y_2O_2CO_3$ at 300 °C.[11] In agreement with our findings, phase diagrams published by Chai et al. showed the formation of $Ln_2O_2CO_3$ at temperatures as low as 250 °C.[39]

X-ray diffraction patterns of powders obtained from **4** after addition of water revealed the presence of praseodymium hydroxy chloride ($Pr(OH)_2Cl$) as well as oxo chloride (PrOCl) (Figure 11). Both phases crystallized as platelets and showed a high tendency for agglomerations (Figure 10e,f). This observation conforms with the formation of lanthanide hydroxyl chloride particles, $RE(OH)_2Cl$, obtained by solvothermal treatment of rare-earth hexahydrates by Hosokawa et al.[42] The formation of a chlorine-containing phase is a consequence of the use of chlorine-containing precursor **4**, revealing the strong influence of the precursor chemistry on materials synthesis, and is conformal with phase assignments based on the mass loss in TG/DTA analysis. The fact that powders obtained from the same precursor decomposed by solvothermal treatment under addition of KOH_{aq} did not contain any crystalline chlorine phase may be explained by a reaction between Cl^- and K^+ ions during the treatment and subsequent removal from the system by the final washing steps.

Influence of the Solvent. To further study the impact of the precursors' molecular structures on the phase and morphology of the resultant materials, the solvothermal decomposition of **1** and **2** was also examined in hexane as a nonpolar solvent (250

DOI: 10.1021/acs.inorgchem.5b00529
Inorg. Chem. 2015, 54, 6267−6280

°C, 24 h). Hereby, a confirmation of the results already obtained for the solvothermal synthesis in isopropyl alcohol was found: The decomposition in hexane in the presence of KOH_{aq} results in highly crystalline powders (Figure S3, Supporting Information). Herein, the presence of the basic medium (KOH_{aq}) augments the kinetics of both hydrolysis and cross-condensation reactions responsible for formation of −Pr−O−Pr− bridges that is reflected in the high crystallinity of the product as observed in XRD.

Hydrolysis of **1** and **2** in the presence of 1 molar equiv of water led to $Pr(OH)_3$ nanoparticles only 5−10, respectively 15−20 nm, in diameter (Figures S4a and S5a,c, Supporting Information). The addition of 5 molar equiv of water induced the formation of mostly amorphous products as obvious from both XRD (Figure S4b) and TEM (Figure S5b,d). Around neutral pH, the driving force for cross-condensation reactions is low, resulting in highly agglomerated particles; since not all praseodymium centers are able to form hydroxide structures, the formation of hydroxo-bridged structures is a logical consequence. The found tendency for the formation of amorphous and agglomerated powders upon solvothermal treatment in hexane after activation with water is in contrast to our previous observations on powders obtained when isopropyl alcohol was used as the solvent. Two aspects that may influence the materials formation have to be considered in this context: first, the different polarities of hexane and isopropyl alcohol and, second, the different vapor pressures of the two solvents. Due to their different polarities, water used as the activation agent is not miscible with hexane, while the use of isopropyl alcohol supports the hydrolysis of the precursor due to their complete miscibility and the presence of hydroxyl groups in the alcohol that facilitates the ligand-exchange processes. Besides, it has to be taken into account that secondary alcohols, thus isopropyl alcohol, undergo controlled dehydration upon solvothermal treatment at elevated temperatures, resulting in the formation of additional water, which then further triggers the hydrolysis of the alkoxide.[43] Therefore, it seems that powders of increased crystallinity can be obtained when isopropyl alcohol is chosen as the solvent in the solvothermal synthesis instead of hexane. Moreover, isopropyl alcohol exhibits a higher vapor pressure at elevated temperatures when compared to hexane (temperature for, e.g., 15 200 mmHg of vapor pressure: isopropyl alcohol, 186.0 °C; hexane, 209.4 °C[44]). Consequently, it is most likely that a higher pressure is built up within the reaction vessel during the solvothermal treatment in isopropyl alcohol than in hexane. In general, the increase in pressure during the solvothermal synthesis induces a higher solubility and reactivity of the reaction species, which is highly beneficial for the formation of crystalline materials. Thus, the lower reaction pressure resulting from the lower vapor pressure of hexane when compared to isopropyl alcohol (under, in other respects—volume, precursor concentration, temperature, activation with water—the same reaction conditions) results in the observed less crystalline powders. Consequently, it becomes obvious that the solvent properties have an influence on the crystallization behavior of the solid material, which reveals the importance of the appropriate solvent choice when aiming for nanocrystalline materials by solvothermal synthesis. Again, the most beautiful example of the influence of the precursor configuration on the phase composition is the formation of $Pr(OH)_2Cl$ when chloro tritox complex **4** is hydrolyzed in hexane (Figure S4). The limited amount of water can knock out the bulky tritox group (less basic than −OH units), yet the substitution of chlorine under the relatively mild conditions of the solvothermal treatment is less favored. As a result, and also due to the high halophilicity of the lanthanide ion, chlorine is incorporated into the lattice of the final material. These findings reveal once more the strong impact of the precursor chemistry on materials formation.

CONCLUSIONS

Four new praseodymium alkoxo and amido compounds ($[Pr_3(\mu_3\text{-}OtBu)_2(\mu_2\text{-}OtBu)_3(OtBu)_4(HOtBu)_2]$ (**1**), $[Pr\{OC(tBu)_3\}_3(THF)]$ (**2**), $[PrCl\{N(SiMe_3)_2\}_2(THF)]_2$ (**3**), and $[PrCl\{OC(tBu)_3\}_2(THF)]_2$ (**4**)) were synthesized and structurally characterized by single-crystal X-ray diffraction analysis. Subsequently, **1**, **2**, and **4** were employed as precursors to investigate the influence of the precursor chemistry on the transformation of source molecules into nanostructured materials. The concept illustrated in this work shows that short-range chemical order present in the precursor compounds can be translated into infinite correlation lengths in three dimensions, making precursor-based approaches an attractive platform for the rational material design and tuning of process parameters beyond the equilibrium regime, which is mostly driven by thermodynamic and entropic considerations. It was clearly shown that the molecular structure of the precursor units and the basicity of the chosen ligands strongly influence the decomposition behavior in the bulk phase (TG/DTA) and the eventual formation of the solid phase under solvothermal conditions. This finally led to various morphologies and crystalline phases. Being subject to the original structure and ligand arrangement in the precursor molecule, the appropriate choice of activation agents triggering the hydrolysis of the molecular precursors imposes a control over the morphology and phase of the final material. Thus, praseodymium hydroxide phases ranging from nanorods and platelets to nanoparticles were obtained by the solvothermal treatment of **1**, **2**, and **4**.

ASSOCIATED CONTENT

Supporting Information

Description of the formation of the $Pr_{9.33}Si_6O_{26}$ second phase and materials formation in hexane. The Supporting Information is available free of charge on the ACS Publications website at DOI: 10.1021/acs.inorgchem.5b00529.

AUTHOR INFORMATION

Corresponding Author

*E-mail: sanjay.mathur@uni-koeln.de. Fax: (+)49 221 470 5899. Phone: (+)49 221 470 5627.

Notes

The authors declare no competing financial interest.

ACKNOWLEDGMENTS

We thank the German Science Foundation (DFG) for financial support in the frame of Schwerpunktprogramm SPP-1166 and the University of Cologne for providing infrastructure and financial assistance. We thank Dr. Hao Shen, Technische Universität Braunschweig, for TEM characterization and fruitful discussions.

REFERENCES

(1) (a) Maas, H.; Currao, A.; Calzaferri, G. *Angew. Chem., Int. Ed.* **2002**, *41* (14), 2495−2497. (b) Zou, J. P.; Luo, S. L.; Li, M. J.; Tang, X. H.; Xing, Q. J.; Peng, Q.; Guo, G. C. *Polyhedron* **2010**, *29* (13),

DOI: 10.1021/acs.inorgchem.5b00529
Inorg. Chem. 2015, 54, 6267−6280

2674−2679. (c) Gallardo, H.; Conte, G.; Bortoluzzi, A. J.; Bechtold, I. H.; Pereira, A.; Quirino, W. G.; Legnani, C.; Cremona, M. *Inorg. Chim. Acta* **2011**, *365* (1), 152−158. (d) Edelmann, F. T. *Coord. Chem. Rev.* **2013**, *257* (7−8), 1122−1231. (e) Edelmann, F. T. *Chem. Soc. Rev.* **2012**, *41* (23), 7657−7672.

(2) (a) Soukka, T.; Kuningas, K.; Rantanen, T.; Haaslahti, V.; Lovgren, T. *J. Fluoresc.* **2005**, *15* (4), 513−528. (b) Speghini, A.; Piccinelli, F.; Bettinelli, M. *Opt. Mater.* **2011**, *33* (3), 247−257. (c) Bouzigues, C.; Gacoin, T.; Alexandrou, A. *ACS Nano* **2011**, *5* (11), 8488−8505. (d) Fischer, S.; Gill, V. J.; Kovacs, J.; Miele, P.; Keary, J.; Silcott, V.; Huang, S.; Borio, L.; Stock, F.; Fahle, G.; Brown, D.; Hahn, B.; Townley, E.; Lucey, D.; Masur, H. *J. Infect. Dis.* **2001**, *184* (11), 1485−1488. (e) Hubbard, D. S.; Houlne, M. P.; Kiefer, G.; Janssen, H. F.; Hacker, C.; Bornhop, D. J. *Lasers Med. Sci.* **1998**, *13* (1), 14−21. (f) Jaque, D.; Vetrone, F. *Nanoscale* **2012**, *4* (15), 4301−4326. (g) Licha, K. Contrast agents for optical imaging. In *Contrast Agents II*; Krause, W., Ed.; Springer-Verlag: Berlin, Berlin, 2002; Vol. *222*, pp 1−29. (h) Yam, V. W. W.; Lo, K. K. W. *Coord. Chem. Rev.* **1999**, *184*, 157−240. (i) Mudring, A. V.; Tang, S. F. *Eur. J. Inorg. Chem.* **2010**, *18*, 2569−2581.

(3) (a) Hatano, M.; Ishihara, K. *Chem. Commun.* **2013**, *49* (20), 1983−1997. (b) You, L. X.; Shen, Z. Q.; Kong, J.; Ling, J. *Polymer* **2014**, *55* (10), 2404−2410. (c) Qian, C. W.; Zhang, X. M.; Zhang, Y.; Shen, Q. *J. Organomet. Chem.* **2010**, *695* (5), 747−752. (d) Dioury, F.; Sambou, S.; Guene, E.; Sabatou, M.; Ferroud, C.; Guy, A.; Port, M. *Tetrahedron* **2007**, *63* (1), 204−214. (e) Manning, H. C.; Goebel, T.; Marx, J. N.; Bornhop, D. J. *Org. Lett.* **2002**, *4* (7), 1075−1078. (f) Picard, C.; Geum, N.; Nasso, I.; Mestre, B.; Tisnes, P.; Laurent, S.; Muller, R. N.; Vander Elst, L. *Bioorg. Med. Chem. Lett.* **2006**, *16* (20), 5309−5312. (g) Laurent, S.; Parac-Vogt, T. N.; Kimpe, K.; Thirifays, C.; Binnemans, K.; Muller, R. N.; Elst, L. V. *Eur. J. Inorg. Chem.* **2007**, *14*, 2061−2067. (h) Querol, M.; Bogdanov, A. *J. Magn. Reson. Imaging* **2006**, *24* (5), 971−982. (i) Comby, S.; Imbert, D.; Vandevyver, C.; Bunzli, J. C. G. *Chem.—Eur. J.* **2007**, *13* (3), 936−944.

(4) (a) Mathur, S.; Veith, M.; Shen, H.; Hufner, S.; Jilavi, M. H. *Chem. Mater.* **2002**, *14* (2), 568−582. (b) Mathur, S.; Shen, H.; Veith, M.; Rapalaviciute, R.; Agne, T. *J. Am. Ceram. Soc.* **2006**, *89* (6), 2027−2033. (c) Mathur, S.; Altmayer, J.; Shen, H. *Z. Anorg. Allg. Chem.* **2004**, *630* (12), 2042−2048. (d) Mathur, S.; Veith, M.; Ruegamer, T.; Hemmer, E.; Shen, H. *Chem. Mater.* **2004**, *16* (7), 1304−1312. (e) Hubert-Pfalzgraf, L. G.; Daniele, S. *C. R. Chim.* **2004**, *7* (5), 521−527. (f) Veith, M.; Belot, C.; Huch, V. *Eur. J. Inorg. Chem.* **2012**, *8*, 1218−1228. (g) Mantymaki, M.; Ritala, M.; Leskela, M. *Coord. Chem. Rev.* **2012**, *256* (9−10), 854−877. (h) Kritikos, M.; Moustiakimov, M.; Westin, G. *Inorg. Chim. Acta* **2012**, *384*, 125−132. (i) Cohen, S. M. *Curr. Opin. Chem. Biol.* **2007**, *11* (2), 115−120. (j) Werts, M. H. V.; Woudenberg, R. H.; Emmerink, P. G.; van Gassel, R.; Hofstraat, J. W.; Verhoeven, J. W. *Angew. Chem., Int. Ed.* **2000**, *39* (24), 4542−4544.

(5) (a) Veith, M. *J. Chem. Soc., Dalton Trans.* **2002**, *12*, 2405−2412. (b) John, L.; Sobota, P. *Acc. Chem. Res.* **2014**, *47* (2), 470−481. (c) Seisenbaeva, G. A.; Kessler, V. G. *Nanoscale* **2014**, *6* (12), 6229−6244. (d) Devi, A. *Coord. Chem. Rev.* **2013**, *257* (23−24), 3332−3384.

(6) (a) Hemmer, E.; Kohl, Y.; Colquhoun, V.; Thielecke, H.; Soga, K.; Mathur, S. *J. Phys. Chem. B* **2010**, *114* (12), 4358−4365. (b) Hemmer, E.; Huch, V.; Adlung, M.; Wickleder, C.; Mathur, S. *Eur. J. Inorg. Chem.* **2011**, *13*, 2148−2157. (c) Joulia, A.; Vardelle, M.; Rossignol, S. *J. Eur. Ceram. Soc.* **2013**, *33* (13−14), 2633−2644.

(7) Pearson, R. G. *J. Am. Chem. Soc.* **1963**, *85* (22), 7.

(8) (a) Veith, M.; Mathur, S.; Mathur, C. *Polyhedron* **1998**, *17* (5−6), 1005−1034. (b) Bradley, D. C.; Mehrotra, R. C.; Gaur, D. P. *Metal Alkoxides*; Academic Press: London, New York, San Francisco, 1978.

(9) Boyle, T. J.; Ottley, L. A. M. *Chem. Rev.* **2008**, *108* (6), 1896−1917.

(10) Bradley, D. C.; Chudzynska, H.; Hursthouse, M. B.; Motevalli, M. *Polyhedron* **1991**, *10* (10), 1049−1059.

(11) Veith, M.; Mathur, S.; Kareiva, A.; Jilavi, M.; Zimmer, M.; Huch, V. *J. Mater. Chem.* **1999**, *9* (12), 3069−3079.

(12) Gromada, J.; Mortreux, A.; Chenal, T.; Ziller, J. W.; Leising, F.; Carpentier, J. F. *Chem.—Eur. J.* **2002**, *8* (16), 3773−3788.

(13) Misra, P.; Misra, S. N.; Mehrotra, R. C. *Aust. J. Chem.* **1968**, *21*, 4.

(14) Daniele, S.; Hubert-Pfalzgraf, L. G.; Hitchcock, P. B.; Lappert, M. F. *Inorg. Chem. Commun.* **2000**, *3* (5), 218−220.

(15) Hubert-Pfalzgraf, L. G.; Daniele, S.; Bennaceur, A.; Daran, J. C.; Vaissermann, J. *Polyhedron* **1997**, *16* (7), 1223−1234.

(16) Mathur, S. S. H. In *Encyclopedia of Nanoscience and Nanotechnology*; Nalwa, H. S., Ed.; American Scientific Publisher: Stevenson Ranch, CA, 2004; Vol. *4*, pp 131−191.

(17) (a) Irfanullah, M.; Iftikhar, K. *J. Fluoresc.* **2011**, *21* (2), 673−686. (b) Radhika, S.; Sreeram, K. J.; Nair, B. U. *J. Chem. Sci.* **2014**, *126* (1), 65−73.

(18) Lo Nigro, R.; Fiorenza, P.; Catalano, M. R.; Fisichella, G.; Roccaforte, F.; Malandrino, G. *Surf. Coat. Technol.* **2013**, *230*, 152−162.

(19) (a) Antoshin, G. V.; Minachev, K. M.; Dmitriev, R. V. *Russ. Chem. Bull.* **1967**, *16*, 1793−171795. (b) Asami, K.; Kusakabe, K.; Ashi, N.; Ohtsuka, Y. *Appl. Catal., A* **1997**, *156* (1), 43−56.

(20) (a) Quievryn, C.; Bernard, S.; Miele, P. *Nanomater. Nanotechnol.* **2014**, *4*, 8. (b) Majeed, S.; Shivashankar, S. A. *Mater. Chem. Phys.* **2013**, *143* (1), 155−160. (c) Chandar, N. K.; Jayavel, R. *Mater. Res. Bull.* **2014**, *50*, 417−420.

(21) Bradley, D. C.; Ghotra, J. S.; Hart, F. A. *J. Chem. Soc., Dalton Trans.* **1973**, *10*, 1021−1027.

(22) (a) Bartlett, P. D. L.; E, B. *J. Am. Chem. Soc.* **1955**, *77*, 2804−2805. (b) Wolczanski, P. T. *Polyhedron* **1995**, *14* (22), 3335−3362.

(23) Boyle, T. J.; Bunge, S. D.; Clem, P. G.; Richardson, J.; Dawley, J. T.; Ottley, L. A. M.; Rodriguez, M. A.; Tuttle, B. A.; Avilucea, G. R.; Tissot, R. G. *Inorg. Chem.* **2005**, *44* (5), 1588−1600.

(24) Boyle, T. J.; Ottley, L. A. M.; Brewer, L. N.; Sigman, J.; Clem, P. G.; Richardson, J. J. *Eur. J. Inorg. Chem.* **2007**, *24*, 3805−3815.

(25) Evans, W. J.; Sollberger, M. S.; Hanusa, T. P. *J. Am. Chem. Soc.* **1988**, *110* (6), 1841−1850.

(26) (a) Schuetz, S. A.; Silvernail, C. M.; Incarvito, C. D.; Rheingold, A. L.; Clark, J. L.; Day, V. W.; Belot, J. A. *Inorg. Chem.* **2004**, *43* (20), 6203−6214. (b) Wang, J.; Yao, Y.; Zhang, Y.; Shen, Q. *Inorg. Chem.* **2009**, *48*, 744−751. (c) Veith, M.; Belot, C.; Huch, V. *Inorg. Chem. Commun.* **2012**, *18*, 101−104.

(27) (a) Wang, Y. B.; Luo, Y. J.; Chen, J.; Xue, H. M.; Liang, H. Z. *New J. Chem.* **2012**, *36* (4), 933−940. (b) Sinenkov, M.; Kirillov, E.; Roisnel, T.; Fukin, G.; Trifonov, A.; Carpentier, J. F. *Organometallics* **2011**, *30* (20), 5509−5523. (c) Boyle, T. J.; Steele, L. A. M.; Burton, P. D.; Hoppe, S. M.; Lockhart, C.; Rodriguez, M. A. *Inorg. Chem.* **2012**, *51* (22), 12075−12092.

(28) Wedler, M.; Gilje, J. W.; Pieper, U.; Stalke, D.; Noltemeyer, M.; Edelmann, F. T. *Chem. Ber.* **1991**, *124* (5), 1163−1165.

(29) Stecher, H. A.; Sen, A.; Rheingold, A. L. *Inorg. Chem.* **1989**, *28* (17), 3280−3282.

(30) Herrmann, W. A.; Anwander, R.; Kleine, M.; Scherer, W. *Chem. Ber./Recl.* **1992**, *125* (9), 1971−1979.

(31) Van den Hende, J. R.; Hitchcock, P. B.; Lappert, M. F. *J. Chem. Soc., Dalton Trans.* **1995**, *13*, 2251−2258.

(32) (a) Karl, M.; Seybert, G.; Massa, W.; Agarwal, S.; Greiner, A.; Dehnicke, K. *Z. Anorg. Allg. Chem.* **1999**, *625* (9), 1405−1407. (b) Berg, D.; Gendron, R. *Can. J. Chem.* **2000**, *78* (4), 454−458.

(33) (a) Tilley, T. D.; Zalkin, A.; Andersen, R. A.; Templeton, D. H. *Inorg. Chem.* **1981**, *20* (2), 551−554. (b) Aspinall, H. C.; Bradley, D. C.; Hursthouse, M. B.; Sales, K. D.; Walker, N. P. C.; Hussain, B. *J. Chem. Soc., Dalton Trans.* **1989**, *4*, 623−626.

(34) Niemeyer, M. *Z. Anorg. Allg. Chem.* **2002**, *628* (3), 647−657.

(35) (a) Ma, L.; Chen, W. X.; Zhao, J.; Zheng, Y. F. *J. Cryst. Growth* **2007**, *303* (2), 590−596. (b) Wang, X.; Li, Y. D. *Angew. Chem., Int. Ed.* **2002**, *41* (24), 4790−4793.

(36) Sohn, S.; Kwon, Y.; Kim, Y.; Kim, D. *Powder Technol.* **2004**, *142* (2−3), 136−153.

(37) Peng, Z. A.; Peng, X. G. *J. Am. Chem. Soc.* **2002**, *124* (13), 3343−3353.

(38) Peng, Z. A.; Peng, X. G. *J. Am. Chem. Soc.* **2001**, *123* (7), 1389−1395.

DOI: 10.1021/acs.inorgchem.5b00529
Inorg. Chem. 2015, 54, 6267−6280

(39) Chai, B. H. T.; Mroczkowski, S. *J. Cryst. Growth* **1978**, *44* (1), 84−97.
(40) Han, Z. H.; Xu, P.; Ratinac, K. R.; Lu, G. Q. *J. Cryst. Growth* **2004**, *273* (1−2), 248−257.
(41) Tareen, J. A. K.; Kutty, T. R. N. *J. Cryst. Growth* **1980**, *50* (2), 527−532.
(42) (a) Hosokawa, S.; Iwamoto, S.; Inoue, M. *J. Am. Ceram. Soc.* **2007**, *90* (4), 1215−1221. (b) Hosokawa, S.; Iwamoto, S.; Inoue, M. *J. Alloys Compd.* **2006**, *408*, 529−532.
(43) Fanelli, A. J.; Burlew, J. V. *J. Am. Ceram. Soc.* **1986**, *69* (8), C174−C175.
(44) *Handbook of Chemistry and Physics*, 44th ed.; Chemical Rubber Publishing Co.: Cleveland, OH, 1963.

DOI: 10.1021/acs.inorgchem.5b00529
Inorg. Chem. 2015, 54, 6267−6280